APPENDIX CONTENTS

Appendix Figure S1……page 2

Appendix Figure S2……page 5

Appendix Figure S3……page 6

Appendix Figure S4……page 7

Appendix Figure S5……..page 10

Appendix Figure S6……..page 11

Appendix Figure S7……..page 12

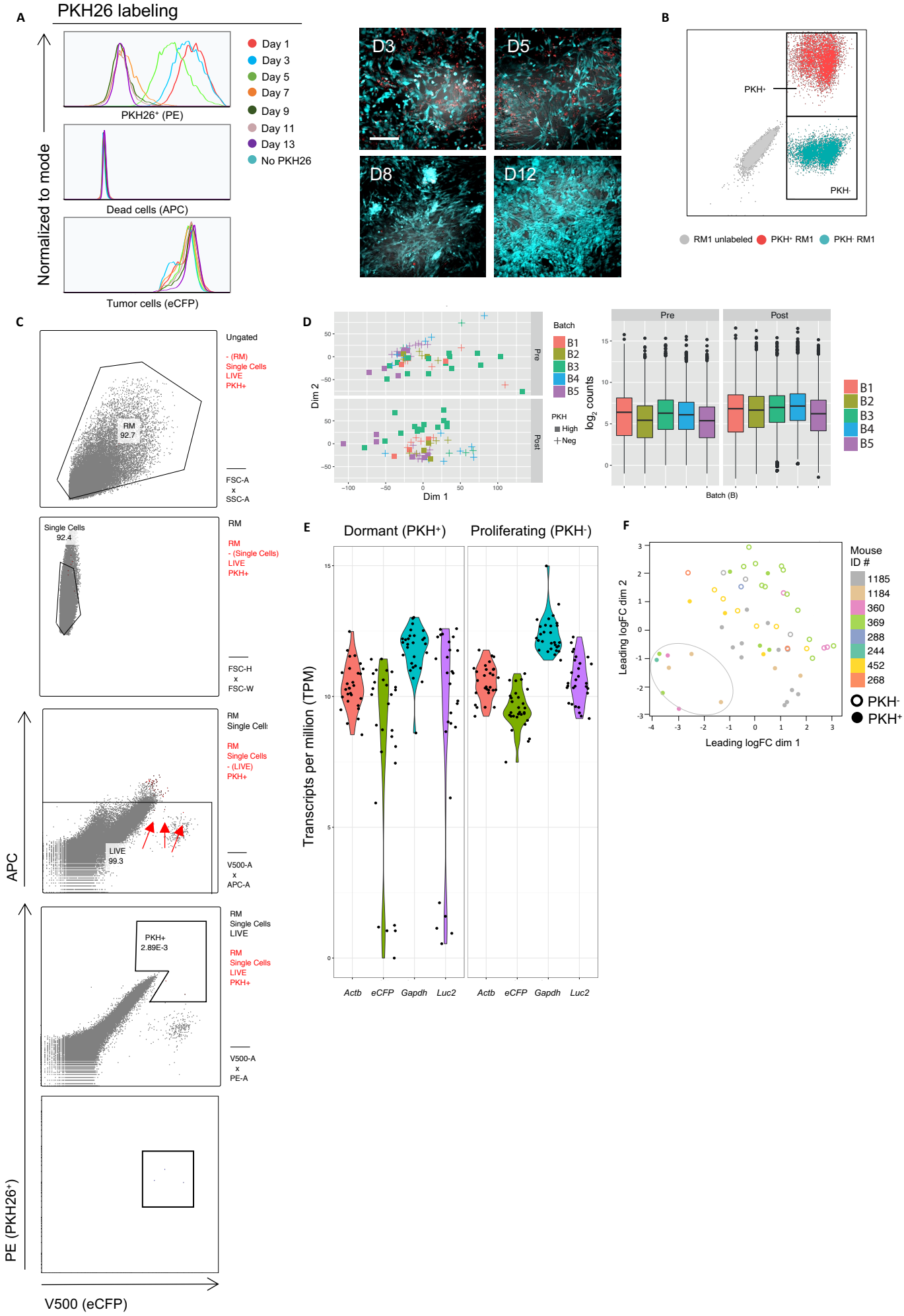
A
PKH26 labeling
Normalized to mode
PKH26⁺ (PE)
Dead cells (APC)
Tumor cells (eCFP)
Day 1
Day 3
Day 5
Day 7
Day 9
Day 11
Day 13
No PKH26
D3
D5
D8
D12
B
PKH⁺
PKH⁻
RM1 unlabeled
PKH⁺ RM1
PKH⁻ RM1
C
Ungated
- (RM)
Single Cells
LIVE
PKH+
RM
92.7
FSC-A
x
SSC-A
Single Cells
92.4
RM
RM
- (Single Cells)
LIVE
PKH+
FSC-H
x
FSC-W
RM
Single Cells
LIVE
99.3
RM
Single Cells
- (LIVE)
PKH+
V500-A
x
APC-A
APC
PKH+
2.89E-3
RM
Single Cells
LIVE
RM
Single Cells
LIVE
PKH+
V500-A
x
PE-A
PE (PKH26⁺)
V500 (eCFP)
D
Batch
B1
B2
B3
B4
B5
PKH
High
Neg
Pre
Post
Dim 1
Dim 2
log2 counts
Batch (B)
E
Dormant (PKH⁺)
Proliferating (PKH⁻)
Transcripts per million (TPM)
Actb
eCFP
Gapdh
Luc2
F
Mouse ID #
1185
1184
360
369
288
244
452
268
PKH⁻
PKH⁺
Leading logFC dim 1
Leading logFC dim 2

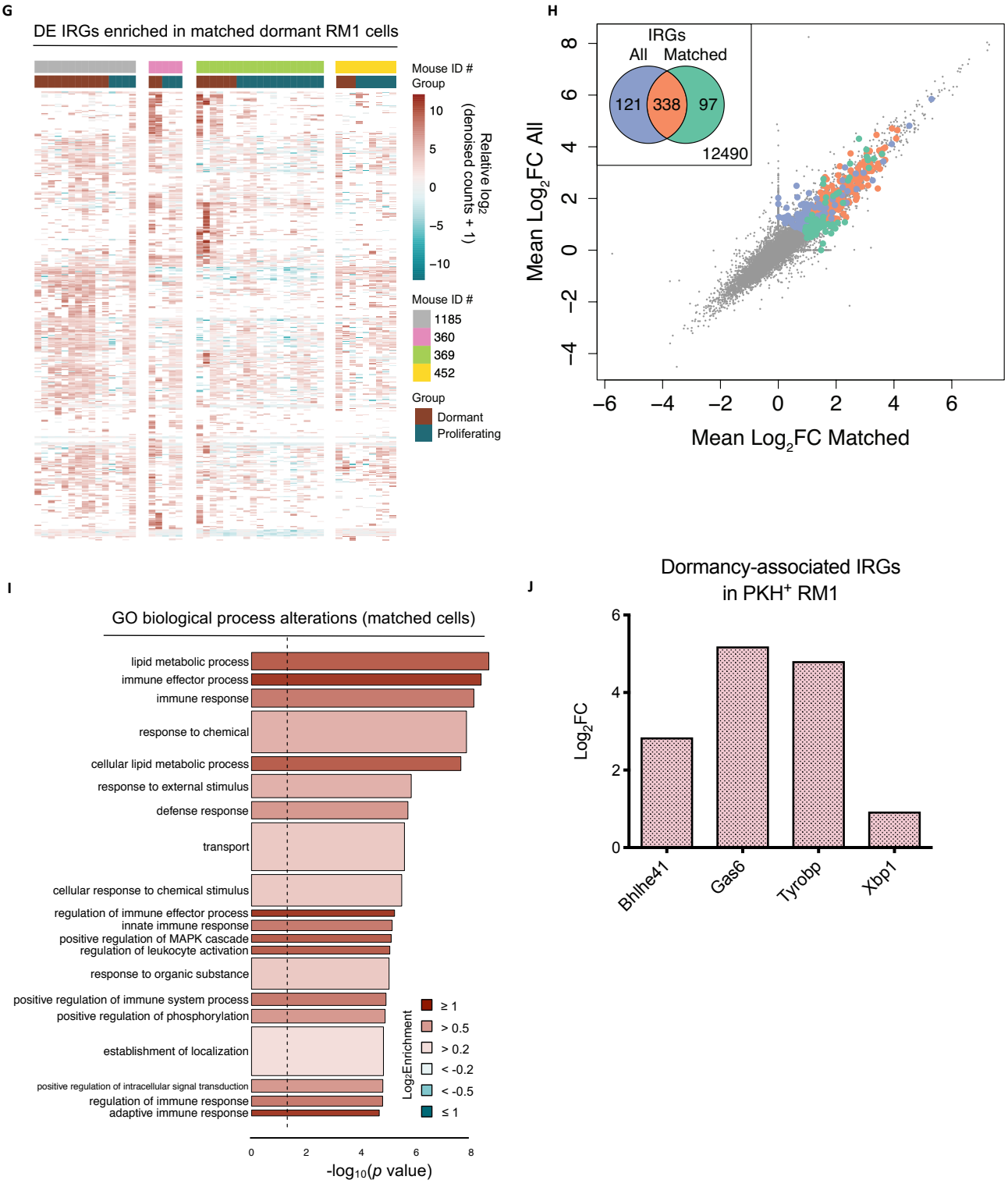
G
DE IRGs enriched in matched dormant RM1 cells
Mouse ID #
Group
10
5
0
−5
−10
Relative log2 (denoised counts + 1)
Mouse ID #
1185
360
369
452
Group
Dormant
Proliferating
H
IRGs
All
Matched
121
338
97
12490
Mean Log2FC All
Mean Log2FC Matched
I
GO biological process alterations (matched cells)
lipid metabolic process
immune effector process
immune response
response to chemical
cellular lipid metabolic process
response to external stimulus
defense response
transport
cellular response to chemical stimulus
regulation of immune effector process
innate immune response
positive regulation of MAPK cascade
regulation of leukocyte activation
response to organic substance
positive regulation of immune system process
positive regulation of phosphorylation
establishment of localization
positive regulation of intracellular signal transduction
regulation of immune response
adaptive immune response
Log2Enrichment
≥ 1
> 0.5
> 0.2
< -0.2
< -0.5
≤ 1
-log10(p value)
J
Dormancy-associated IRGs in PKH+ RM1
Log2FC
Bhlhe41
Gas6
Tyrobp
Xbp1

Appendix Figure S1 Type I IFN signaling is retained in dormant PCa cells in bone metastases
Optimization of PKH26 labeling of RM1 (eCFP/luc2$^+$) parental cells and isolation of bone-derived PKH26$^{+/-}$ single cells for RNAseq. Time course of PKH26 retention in RM1 parental cells by (A) flow cytometry (left) and confocal microscopy (right) at days (*D*) indicated. RM1 cells are eCFP (V500) and PKH26 (PE) positive and live RM1 cells are APC negative. Scale bar, 50 μm. (B) Representative FACS plot and (C) dormant (PKH/PE$^+$) cell detection back-gating of live (APC$^-$) RM1 (V500$^+$) cells. Live dormant (APC$^-$/V500$^+$/PKH$^+$) RM cells are indicated by red arrows and represented as red 'dots' within back-gating plots. (D) PCA clustering of dormant and proliferating RM1 populations pre- and post-normalization with box plots of the distributions of $\log_2$ counts shown (right). (E) Transcript profiles of RM1-specific reporter genes cerulean (*eCFP*) and *luc2* expressed in individual dormant and proliferating RM1 cells. *Actb* and *Gapdh* housekeeper controls shown. (F) Multidimensional scaling (MDS) plot of $\log_2$(denoised counts + 1) from all dormant and proliferating cells, using *plotMDS* (limma). (G) Heatmap of BASiCS-derived $\log_2$(denoised counts + 1) for type I IRGs (upregulated > 2-fold in the INTERFEROME) that are differentially expressed between matched dormant and active populations from the same mice. Only IRGs with no residual over-dispersion shown. Samples with zero counts for individual genes are represented in white. Mice numbers (#) indicated. (H) Dot plot of mean $\log_2$fold change (FC) for DEGs enriched in all dormant cells versus dormant cells from hosts with matched proliferating RM1 cells. Type I IRGs shown in color with overlapping and unique IRGs indicated on the Venn inset. (I) *goana* GO analysis (limma) of DE genes enriched in matched PKH$^{+/-}$ cells from individual mice (n = 4; 22 dormant RM1 cells; 26 proliferating RM1 cells). Gene sets appear in order of significance (p value) with color representing FE and bar width indicating the number of genes in each process. (J) $\log_2$FC of IRGs enriched in PKH$^+$ cells specifically linked to dormancy.

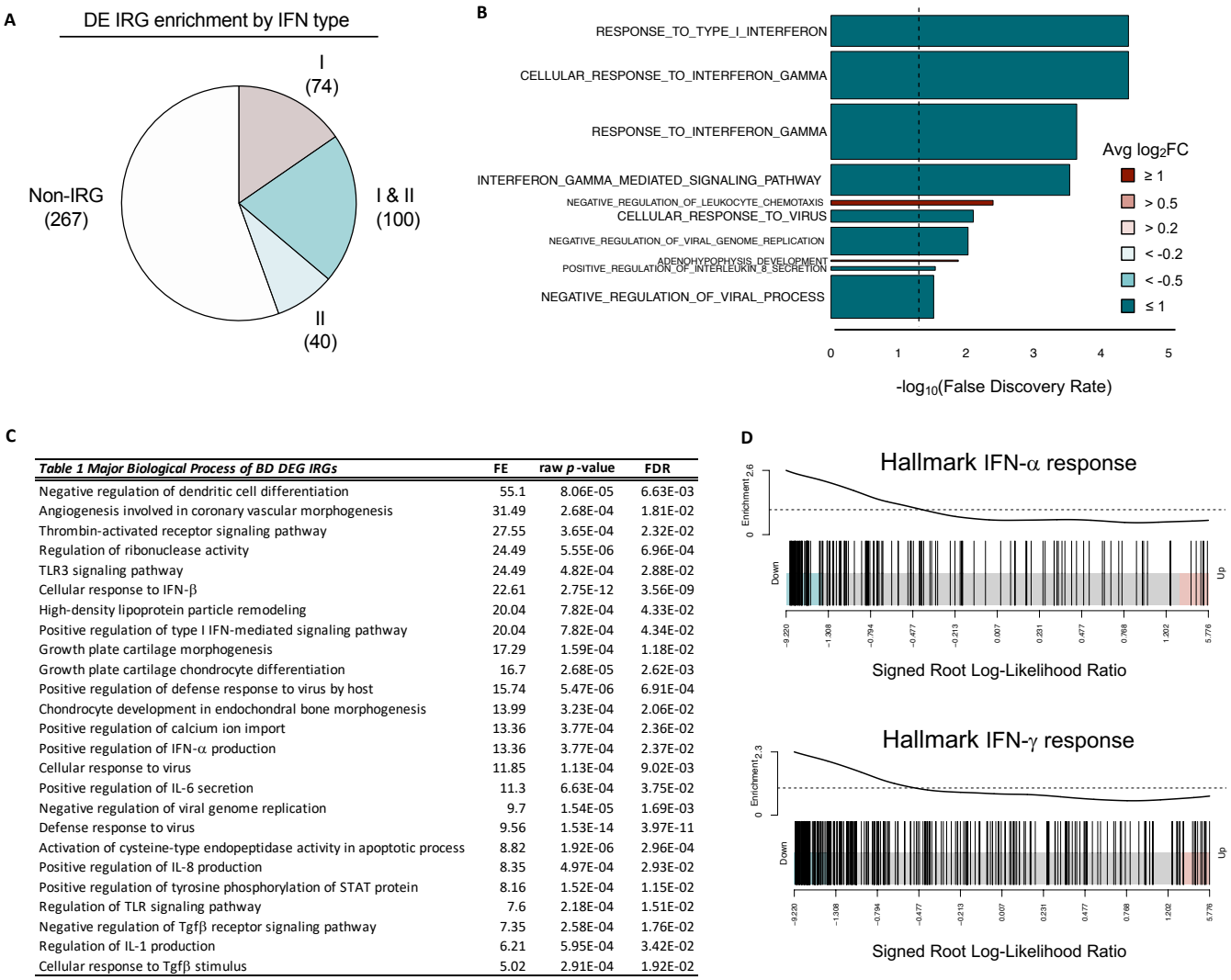

C

Table 1 Major Biological Process of BD DEG IRGs	FE	raw *p* -value	FDR
Negative regulation of dendritic cell differentiation	55.1	8.06E-05	6.63E-03
Angiogenesis involved in coronary vascular morphogenesis	31.49	2.68E-04	1.81E-02
Thrombin-activated receptor signaling pathway	27.55	3.65E-04	2.32E-02
Regulation of ribonuclease activity	24.49	5.55E-06	6.96E-04
TLR3 signaling pathway	24.49	4.82E-04	2.88E-02
Cellular response to IFN-β	22.61	2.75E-12	3.56E-09
High-density lipoprotein particle remodeling	20.04	7.82E-04	4.33E-02
Positive regulation of type I IFN-mediated signaling pathway	20.04	7.82E-04	4.34E-02
Growth plate cartilage morphogenesis	17.29	1.59E-04	1.18E-02
Growth plate cartilage chondrocyte differentiation	16.7	2.68E-05	2.62E-03
Positive regulation of defense response to virus by host	15.74	5.47E-06	6.91E-04
Chondrocyte development in endochondral bone morphogenesis	13.99	3.23E-04	2.06E-02
Positive regulation of calcium ion import	13.36	3.77E-04	2.36E-02
Positive regulation of IFN-α production	13.36	3.77E-04	2.37E-02
Cellular response to virus	11.85	1.13E-04	9.02E-03
Positive regulation of IL-6 secretion	11.3	6.63E-04	3.75E-02
Negative regulation of viral genome replication	9.7	1.54E-05	1.69E-03
Defense response to virus	9.56	1.53E-14	3.97E-11
Activation of cysteine-type endopeptidase activity in apoptotic process	8.82	1.92E-06	2.96E-04
Positive regulation of IL-8 production	8.35	4.97E-04	2.93E-02
Positive regulation of tyrosine phosphorylation of STAT protein	8.16	1.52E-04	1.15E-02
Regulation of TLR signaling pathway	7.6	2.18E-04	1.51E-02
Negative regulation of Tgfβ receptor signaling pathway	7.35	2.58E-04	1.76E-02
Regulation of IL-1 production	6.21	5.95E-04	3.42E-02
Cellular response to Tgfβ stimulus	5.02	2.91E-04	1.92E-02

Appendix Figure S2 Intrinsic type I IFN pathways are specifically suppressed in proliferating PCa cells from bone (A) INTERFEROME database classification of differentially expressed (DE) genes retained in proliferating RM cells compared to parental cells into type I and/or II IFN regulated genes (IRGs). (B) Most significant gene ontology (GO) biological processes from the Broad MSigDB c5 GO gene set collection associated with bone metastasis compared to parental cells. Bar length is the $-\log_{10}$FDR (false discovery rate). Color indicates the mean $\log_2$fold change (FC) of all genes in the gene set and bar width indicates relative gene set size. The dashed line represents FDR = 0.05. (C) Major biological processes enriched in DE IRGs in RM1 (PKH^-) cells derived from bone compared to parental RM1 cells determined by PANTHER analysis. Significance was determined by Fisher's Exact test with FDR (< 0.05) multiple test correction. (D) Barcode plot of the Hallmark IFN-α and -γ response gene sets using the signed log-likelihood ratio statistic from edgeR for bone metastases-derived cells versus lung. Bars indicate statistic value for each gene in the gene set.

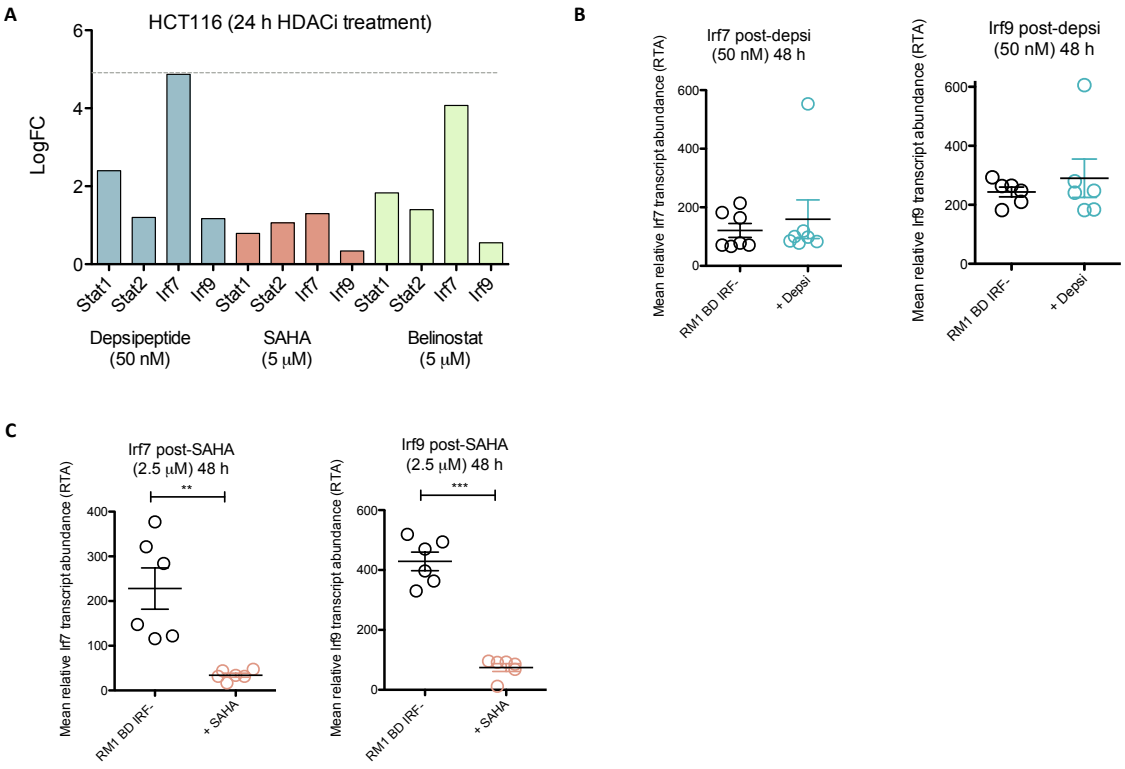

Appendix Figure S3 Loss of tumor-intrinsic type I IFN is inducible by bone marrow cells and is reversed through HDACi modulation (A) Microarray analysis of log_2FC IFN-pathway gene expression values following ± 24 h treatment of HCT116 cells with HDACi Depsipeptide (50 nM; blue), SAHA (5 mM; orange) and Belinostat (5 mM; green) (*n* = 1). qRT-PCR of *Irf7* and *Irf9* expression in RM1 BD Irf$^-$ cells following ± 48 h treatment with selective class I HDACi (B) depsipeptide or (C) pan-HDACi SAHA. Values are means ± SEM of three independent experiments. *p* values represented as * < 0.05, ** < 0.005 and *** < 0.0005 (Student's *t* test). All error bars ± SEM.

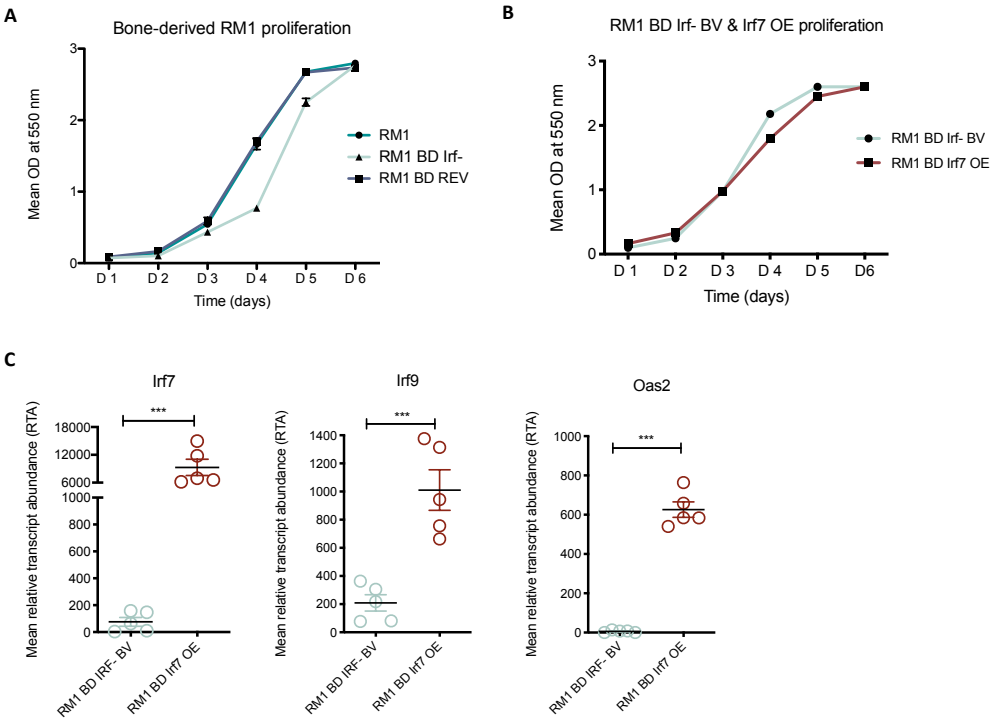
A
Bone-derived RM1 proliferation
Mean OD at 550 nm
Time (days)
RM1
RM1 BD Irf-
RM1 BD REV
B
RM1 BD Irf- BV & Irf7 OE proliferation
Mean OD at 550 nm
Time (days)
RM1 BD Irf- BV
RM1 BD Irf7 OE
C
Irf7
Irf9
Oas2
Mean relative transcript abundance (RTA)
RM1 BD IRF- BV
RM1 BD Irf7 OE

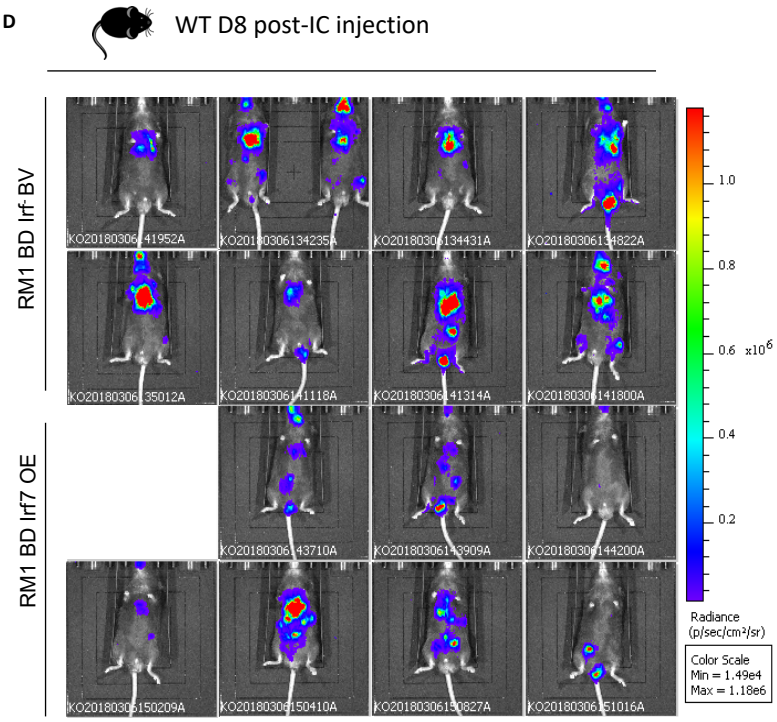
D
WT D8 post-IC injection
RM1 BD Irf-BV
RM1 BD Irf7 OE
Radiance (p/sec/cm²/sr)
Color Scale
Min = 1.49e4
Max = 1.18e6

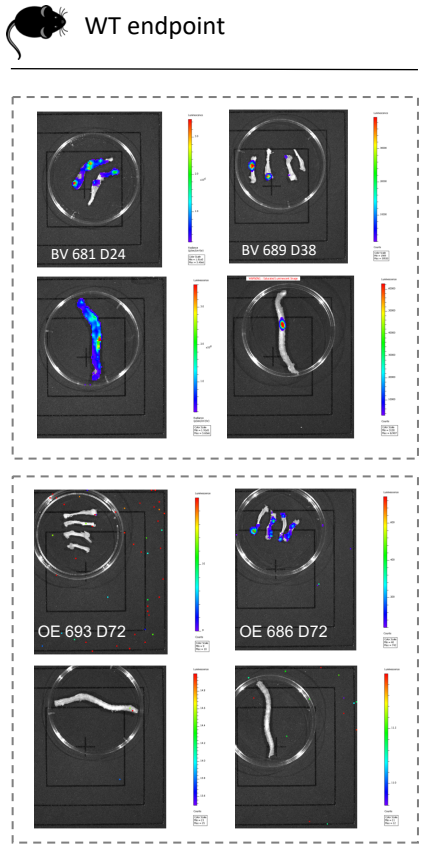
E
WT endpoint
BV 681 D24
BV 689 D38
OE 693 D72
OE 686 D72

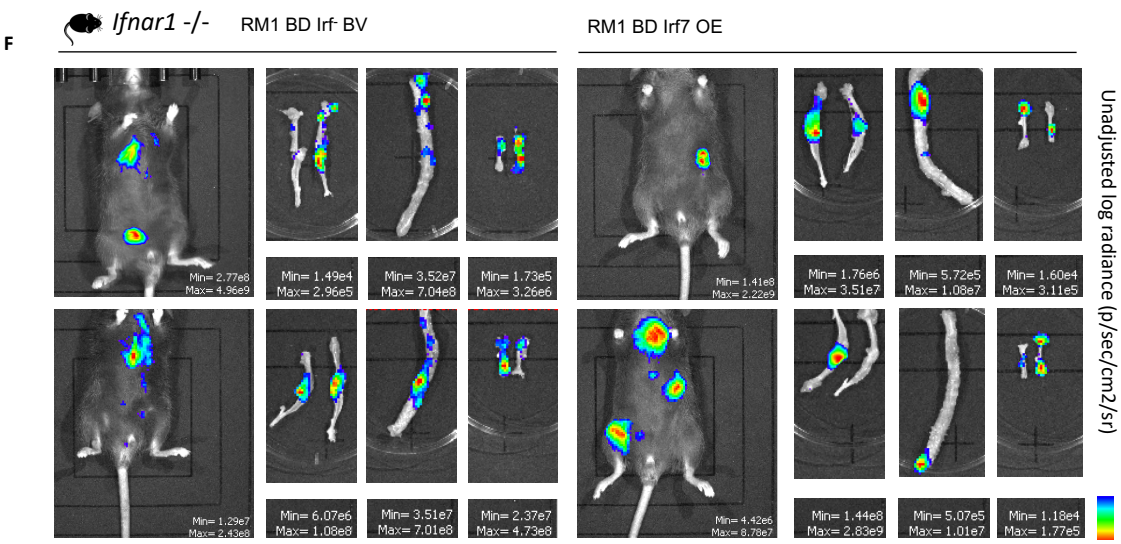

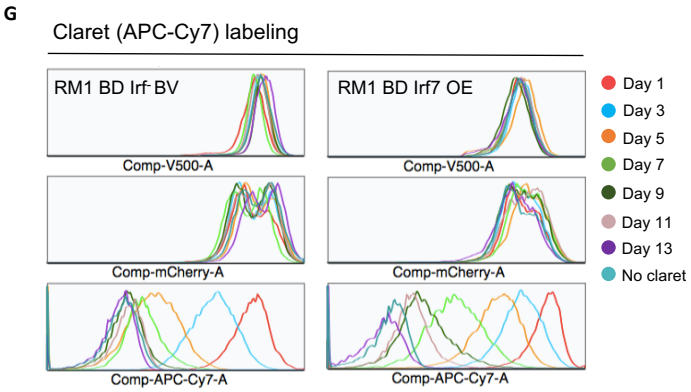

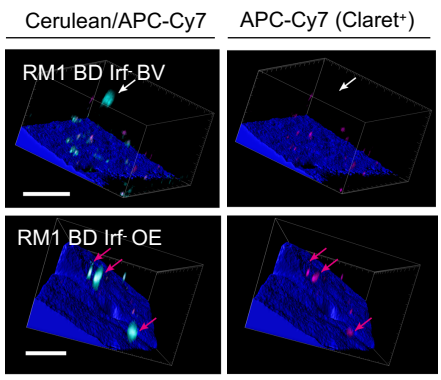

White arrows - active colony (APC-Cy7-)
Magenta arrows - dormant cells (APC-Cy7+)
Blue – rendered bone surface

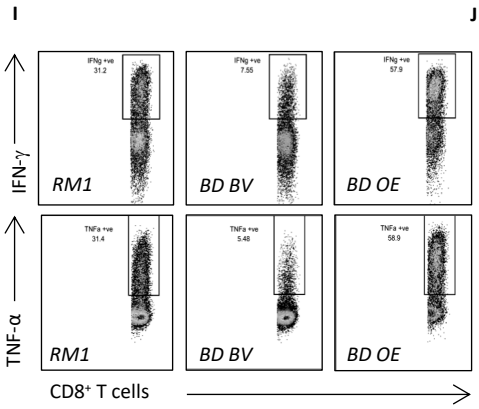

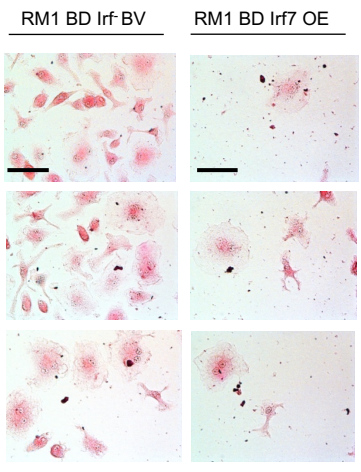

+ naïve BM
+ m-CSF (50 ng/ml)

Appendix Figure S4 Impact of differential tumor-intrinsic IFN signaling on metastasis, dormancy and bone remodeling (A) Proliferation over time (days; D) in RM1 parental cells, RM1 bone-derived Irf-low cells (RM1 BD Irf$^-$) and reverted bone-derived late-passage (LP) cells (RM1 BD REV) determined by SRB assay. Mean optical density (OD) measured at 550 nm. (B) SRB assay of proliferation in RM1 BD Irf$^-$ base-vector (BV) and Irf7 overexpressing (OE) cell lines over 6 days. Mean OD measured at 550 nm. (C) qRT-PCR of *Irf7, Irf9* and *Oas2* upregulation in RM1 BD Irf7 OE compared to RM1 BD Irf$^-$ BV cells (n = 5). (D) Whole mouse bioluminescence imaging showing signal in all but one animal at day 8 post-IC injection of RM1 BD Irf$^-$ BV (n = 9) and RM1 BD Irf7 OE (n = 7) cells. (E) Representative bioluminescence endpoint (D24-72) imaging of legs and spines from RM1 BD Irf$^-$ BV and RM1 BD Irf7 OE tumor-bearing mice. (F) Representative bioluminescence endpoint (D9-12) imaging of whole mouse, legs (representative images shown in Fig 4E), humerus and spines from RM1 BD Irf$^-$ BV and RM1 BD Irf7 OE tumor-bearing *Ifnar1* -/- mice. (G) FACS time course of claret (APC-Cy7) label retention in eCFP/mCherry$^+$ RM1 BD Irf$^-$ BV and RM1 BD Irf7 OE cells. (H) Multiphoton detection of dormant (cerulean (eCFP)/claret$^+$) and proliferating (eCFP$^+$) cells in whole bone at day 17 post-IC injection of RM1 BD Irf$^-$ and RM1 BD Irf7 OE cells (n = 4 per group). White arrows indicate proliferating (APC-Cy7$^-$) colonies. Magenta arrows indicate dormant (APC-Cy7$^+$) single cells. Blue represents rendered bone surface. Scale bars, 50 μm. (I) Representative FACS plots of IFN-γ^+ and TNF-α^+ CD8$^+$ T cells (%) post-ICS induction of T cell (spleen-derived from tumor-bearing mice) activation by RM1 parental, RM1 BD Irf$^-$ BV and RM1 BD Irf7 OE cells (n = 3 per condition/group). (J) Representative TRAP-staining of triplicate-plated osteoclasts differentiated with M-CSF in co-culture with RM1 BD Irf$^-$ and RM1 BD Irf7 OE cells (n = 3 per condition; main representative images shown in Fig 4K). Scale bar, 100 μm. p values represented as *** < 0.0005 (Student's t test). All error bars ± SEM.

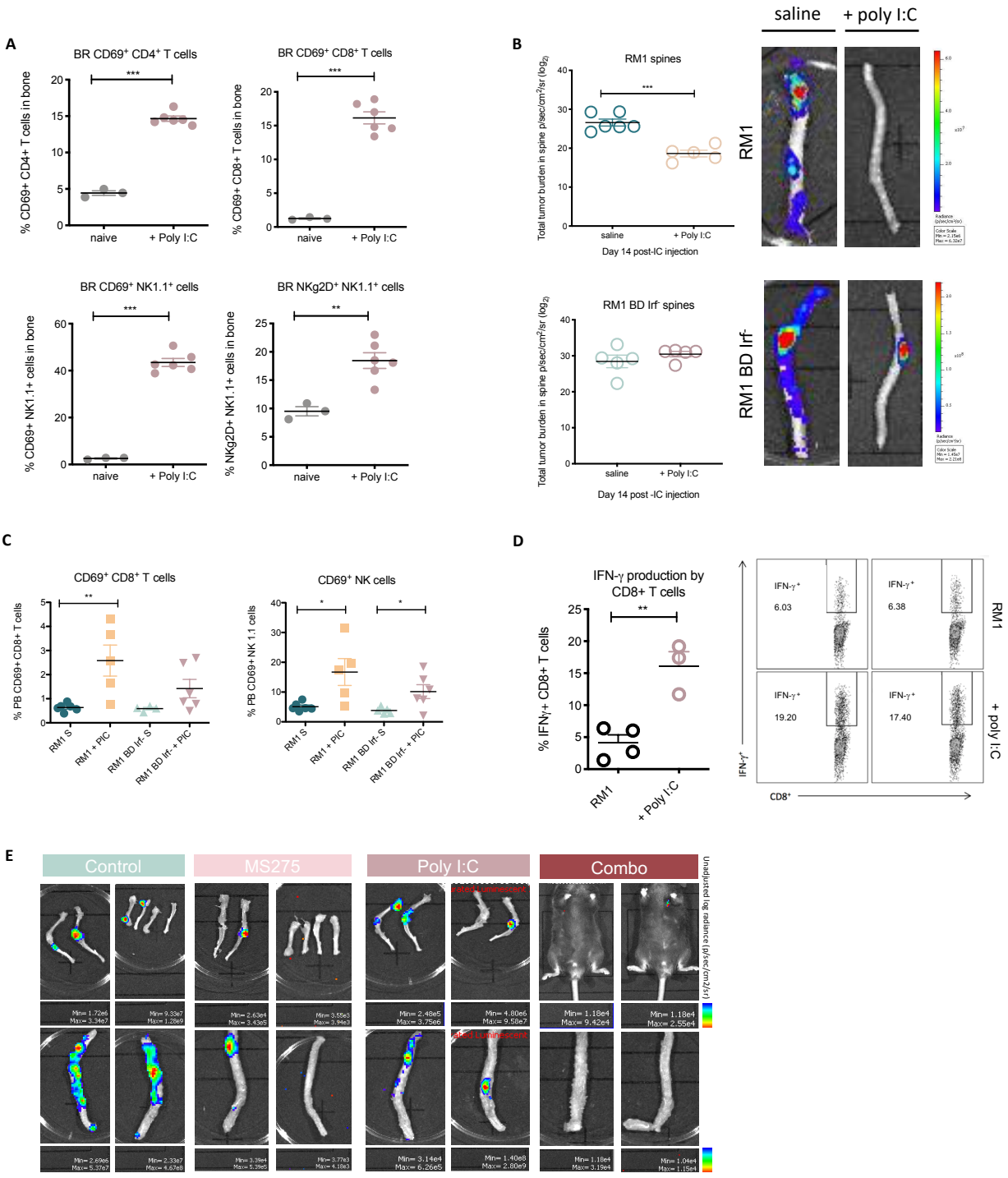

Appendix Figure S5 Bone metastasis is inhibited by therapeutic induction of cell-intrinsic (HDACi) and systemic type I IFN and promotes long-term immune reactivity (A) FACS analysis of immune activation of bone-resident (BR) cells derived from femur, spine, tibia and humerus post-24 h *in vivo* poly I:C treatment (25 mg/mouse) in non-tumor bearing C57BL/6 mice (n = 3). (B) Tumor burden in spine at day 14 post-IC injection of RM1 parental and RM1 BD Irf$^-$ cells as measured by bioluminescent intensity score ($\log_2$ p/sec/cm^2/sr) with values < 4.0x10^4 representing zero burden (n = 5 per group). (C) FACS analysis of peripheral blood (PB) CD8$^+$ T cell and NK cell activation at day 8 post-IC injection of RM1 parental and RM1 BD Irf$^-$ cells. (D) FACS analysis of IFN-γ$^+$ CD8$^+$ T cells (%) post-ICS induction of T cell activation by RM1 parental cells ± poly I:C (n = 3 per condition). (E) Representative bioluminescence endpoint (D9-42) imaging of whole mouse and/or legs and spines from RM1 BD Irf$^-$ animals ± MS275, poly I:C or combination treatment from day 3 post-IC injection (n = 6 per group). p values represented as ** < 0.005 and *** < 0.0005 (Student's t test). All error bars ± SEM.

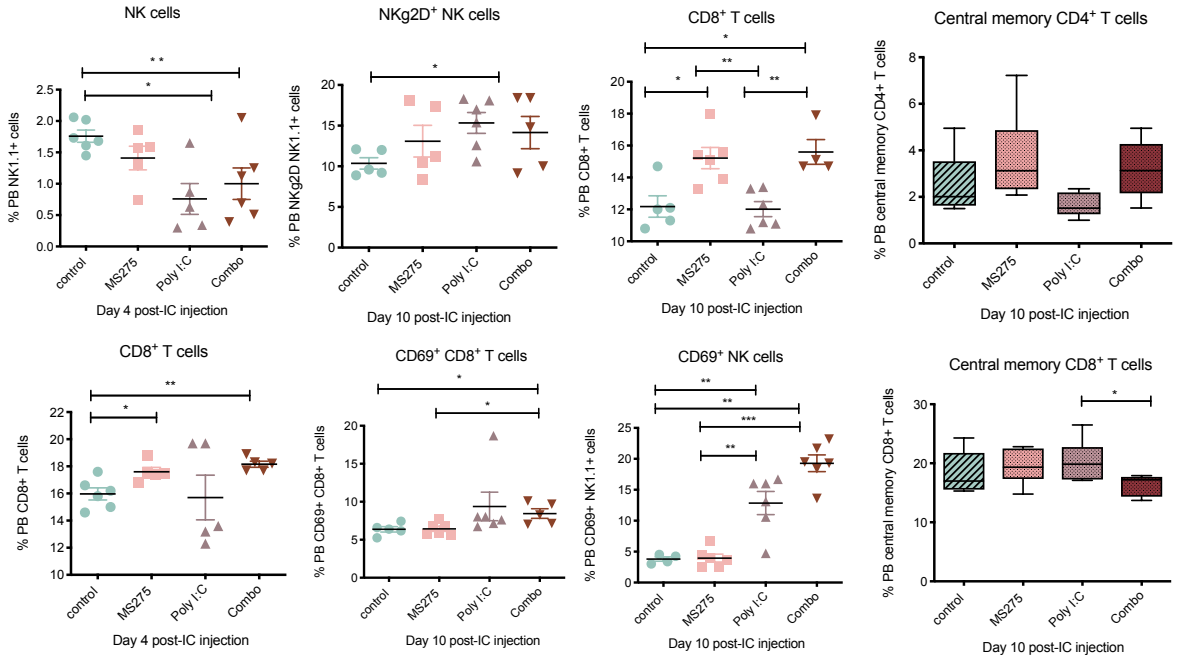

Appendix Figure S6 HDACi and systemic IFN induction provides long-term immune protection from bone-metastatic colonization and outgrowth FACS analysis of peripheral blood (PB) lymphocytes (%) at day 4 and 10 post-IC injection of RM1 BD Irf^{-} cells ± MS275, poly I:C or combination treatment (n = 4-6 per group). p values represented as ** < 0.005 and *** < 0.0005 (Student's t test). All error bars ± SEM.

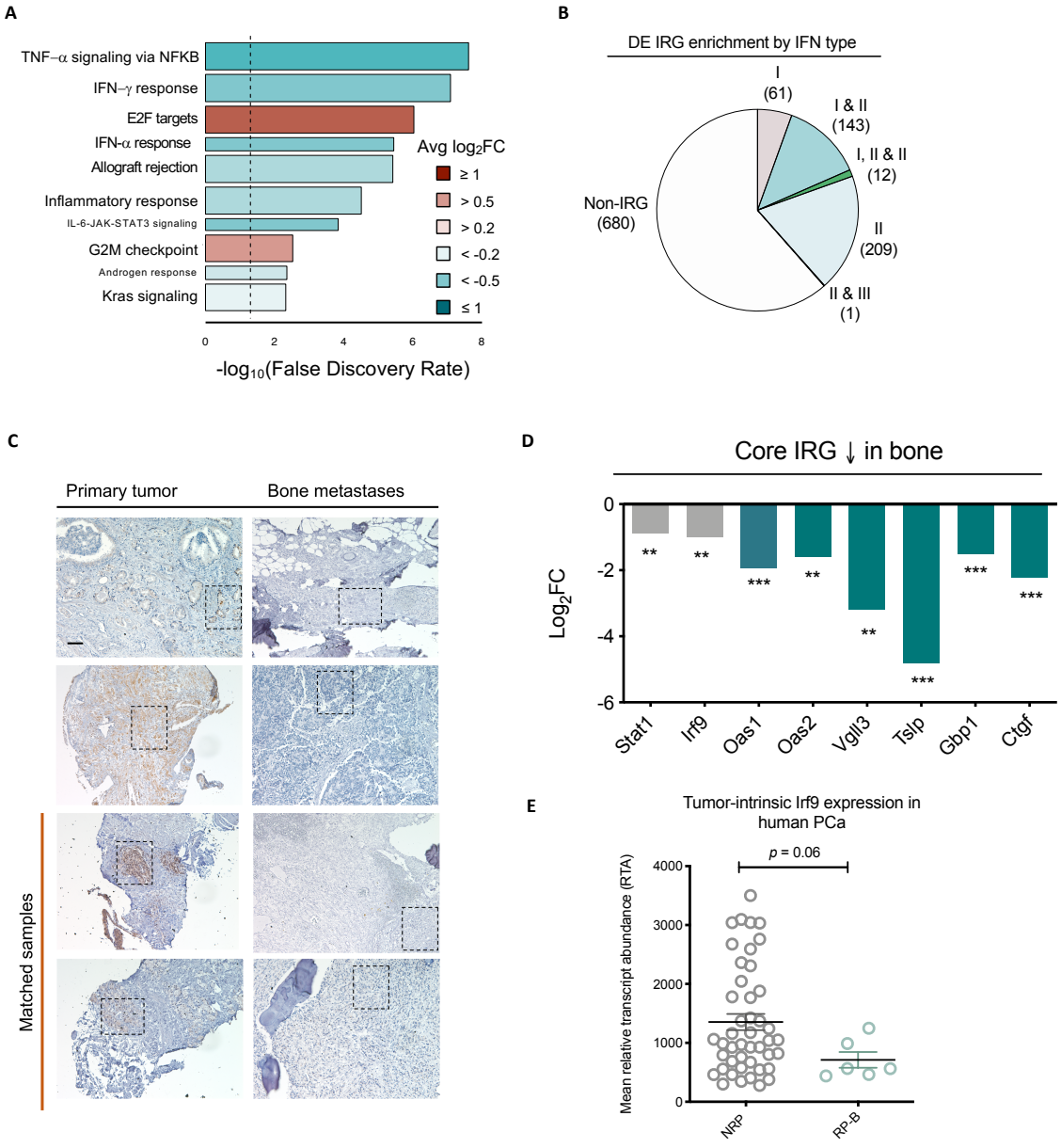

Appendix Figure S7 IFN signaling is decreased in bone-metastatic Pca (A) Hallmark gene set responses associated with bone metastasis by camera analysis. Bar length is the $-\log_{10}$FDR. Color indicates mean $\log_2$FC of all genes in gene set. Bar width is relative gene set size. Dashed line shows FDR = 0.05. (B) Interrogation of suppressed type I, II and III IRGs in bone metastases using the INTERFEROME database. (C) Full-face IHC detection of IRF9 expression in primary prostate tumors and bone metastases with matched samples indicated. IRF9 staining represented by brown (DAB) staining. Scale bar represents 100 μm. Corresponding Fig 7E regions boxed in black. (D) $\log_2$FC of an 8-IRG core signature suppressed in bone metastases, including genes directly involved in IFN-α/β production (grey) and classic downstream targets (blue). GLM by edgeR. (E) Primary tumor-intrinsic expression of *Irf9* in non-recurrent primaries (NRP; n = 45) and recurrent primaries with bone metastases (RP-B; n = 6) from the St Vincent's-Garvan Clinical cohort (Gleason scores >7). Significance (p = 0.06) determined by Mann-Whitney U test.